Multimodal CEA-Targeted Image-Guided Colorectal Cancer Surgery using ^{111}In-Labeled SGM-101

Jan Marie de Gooyer[1,2], Fortuné M.K. Elekonawo[1,2], Desirée L. Bos[1], Rachel S. van der Post[3], André Pèlegrin[4], Bérénice Framery[5], Françoise Cailler[5], Alexander L. Vahrmeijer[6], Johannes H.W. de Wilt[2], and Mark Rijpkema[1]

ABSTRACT

Purpose: Intraoperative image guidance may aid in clinical decision-making during surgical treatment of colorectal cancer. We developed the dual-labeled carcinoembryonic antigen–targeting tracer, [^{111}In]In-DTPA-SGM-101, for pre- and intraoperative imaging of colorectal cancer. Subsequently, we investigated the tracer in preclinical biodistribution and multimodal image-guided surgery studies, and assessed the clinical feasibility on patient-derived colorectal cancer samples, paving the way for rapid clinical translation.

Experimental Design: SGM-101 was conjugated with p-isothiocyanatobenzyl–diethylenetriaminepentaacetic acid (DTPA) and labeled with Indium-111 (^{111}In). The biodistribution of 3, 10, 30, and 100 μg [^{111}In]In-DTPA-SGM-101 was assessed in a dose escalation study in BALB/c nude mice with subcutaneous LS174T human colonic tumors, followed by a study to determine the optimal timepoint for imaging. Mice with intraperitoneal LS174T tumors underwent micro-SPECT/CT imaging and fluorescence image–guided resection. In a final translational experiment, we incubated freshly resected human tumor specimens with the tracer and assessed the tumor-to-adjacent tissue ratio of both signals.

Results: The optimal protein dose of [^{111}In]In-DTPA-SGM-101 was 30 μg (tumor-to-blood ratio, 5.8 ± 1.1) and the optimal timepoint for imaging was 72 hours after injection (tumor-to-blood ratio, 5.1 ± 1.0). In mice with intraperitoneal tumors, [^{111}In]In-DTPA-SGM-101 enabled preoperative SPECT/CT imaging and fluorescence image–guided resection. After incubation of human tumor samples, overall fluorescence and radiosignal intensities were higher in tumor areas compared with adjacent nontumor tissue ($P < 0.001$).

Conclusions: [^{111}In]In-DTPA-SGM-101 showed specific accumulation in colorectal tumors, and enabled micro-SPECT/CT imaging and fluorescence image–guided tumor resection. Thus, [^{111}In]In-DTPA-SGM-101 could be a valuable tool for preoperative SPECT/CT imaging and intraoperative radio-guided localization and fluorescence image–guided resection of colorectal cancer.

Introduction

Colorectal cancer is currently the second leading cause of cancer-related death in women, and the third most common cause in men (1). While therapeutic strategies have evolved throughout the last decades, radical surgical resection of all tumor tissue with clear margins (R0) remains the mainstay of treatment. Surgical treatment has become increasingly versatile with procedures such as cytoreductive surgery for colorectal peritoneal metastasis or extensive exenterative surgery for locally advanced or recurrent rectal cancer (2, 3). Complete tumor resection is pivotal for successful treatment outcome, but remains challenging in many patients. In rectal cancer, involvement of the circumferential resection margin still occurs in 1%–28% of all surgically treated cases (4). There are several factors that can complicate surgical treatment, such as distorted pelvic anatomy after previous resections, multifocal tumor deposits, the presence of multiple small tumor nodules in peritoneally metastasized cancers, and difficulty to distinguish benign from malignant tissue, for example, after neoadjuvant therapy (5). Real-time intraoperative margin assessment and tumor visualization techniques guiding the surgeon may be advantageous to overcome these obstacles.

Carcinoembryonic antigen (CEA)-targeted fluorescence imaging is a technique that can be of added value in surgical treatment of both locoregional and metastasized colorectal cancer. CEA is a widely known glycoprotein and tumor marker that is highly expressed on almost all (more than 95%) colorectal cancers, and also on a variety of other malignancies such as gastric, pancreatic, lung, breast, and esophageal cancer (6). SGM-101 is a CEA-specific chimeric antibody conjugated to a near-infrared (NIR) fluorophore that has been developed to facilitate CEA-targeted fluorescence image–guided surgery of colorectal cancer (7).

Preclinical toxicology, pharmacology, and pharmacokinetic results have demonstrated the absence of significant adverse effects of SGM-101 at doses well above the anticipated maximal human exposure (8). A previous phase I/II clinical trial has also already shown the potential of SGM-101 for intraoperative detection of colorectal cancer tissue. In this trial, CEA-targeted fluorescence-guided surgery resulted in the detection of additional malignant lesions that were not clinically suspected, emphasizing the potential of SGM-101 for intraoperative tumor detection of colorectal cancer (9).

While the use of targeted NIR fluorescence-guided surgery is of great value to enhance oncological procedures, the limited tissue

[1]Department of Radiology, Nuclear Medicine & Anatomy, Radboud University Medical Center, Nijmegen, Gelderland, the Netherlands. [2]Department of Surgical Oncology, Radboud University Medical Center, Nijmegen, Gelderland, the Netherlands. [3]Department of Pathology, Radboud University Medical Center, Nijmegen, Gelderland, the Netherlands. [4]IRCM, Institut de Recherche en Cancérologie de Montpellier, INSERM U1194, Université de Montpellier, Institut régional du Cancer de Montpellier, Montpellier, France. [5]SurgiMab, Montpellier, France. [6]Department of Surgery, Leiden University Medical Center, Leiden, the Netherlands.

Note: Supplementary data for this article are available at Clinical Cancer Research Online (http://clincancerres.aacrjournals.org/).

Corresponding Author: Jan Marie de Gooyer, Radboud University Nijmegen Medical Centre, Nijmegen, the Netherlands 6525GA. Phone: 3102-4366-7244; E-mail: Jan-Marie.Gooyer@radboudumc.nl

Clin Cancer Res 2020;26:5934–42

doi: 10.1158/1078-0432.CCR-20-2255

Translational Relevance

With surgical procedures for colorectal cancer becoming more complicated and extensive, adequate localization and delineation of tumors can be arduous for surgeons. Intraoperative dual-modality image-guided surgery with multimodal tracers is a powerful technique that may provide essential information about tumor margins and the location of metastatic lesions. In this study, we report on the synthesis, *in vitro* characterization, *in vivo* testing, and translational evaluation of a novel, multimodal carcinoembryonic antigen (CEA)-targeting tracer for image-guided colorectal cancer surgery. SPECT/CT and fluorescence imaging clearly visualized specific tracer uptake in a colorectal peritoneal carcinomatosis model, which was confirmed by IHC analysis and gamma counting. The translational *ex vivo* incubation study with fresh, surgically derived human peritoneal colorectal cancer deposits showed high tumor-to-background ratios of the fluorescence and radiosignal. These results demonstrate the clinical potential or our multimodal CEA-targeting tracer for image-guided surgery and facilitate rapid clinical implementation, which is currently in progress.

penetration depth of NIR fluorescence light confines application to superficial tumors. Accurate visualization of deeper located tumors is difficult and is only feasible after proper surgical exposure (9). Adding a radiolabel to a tumor-targeting fluorescent tracer may overcome this limitation by facilitating intraoperative radioguidance (10). Such a dual-labeled tracer also enables preoperative imaging with SPECT/CT and straightforward quantification in (pre)clinical research by gamma counting (11). Quantitative assessment of tracer accumulation and subsequent determination of the tumor-to-background ratio is a key determining factor of tumor detectability and sensitivity of the imaging technique, but accurate quantification of NIR fluorescence is difficult and reported values differ widely (12). Thus, a tracer containing both a fluorophore and a gamma radiation–emitting radionuclide may be a powerful approach (13).

In this study, SGM-101 was conjugated to a radiolabel [Indium-111 (^{111}In)] to create the dual-labeled tracer, [^{111}In]In-DTPA-SGM-101. We evaluated the characteristics, immunoreactivity, and stability of this new tracer *in vitro*. Subsequently, we determined the *in vivo* biodistribution, and performed CEA-targeted micro-SPECT and fluorescence image–guided surgery in a CEA-expressing colorectal cancer xenograft model. In a final translational experiment, we investigated this new tracer in an *ex vivo* incubation experiment with patient-derived surgically resected peritoneal colorectal cancer deposits.

Materials and Methods

Synthesis of DTPA-SGM-101

SGM-101 is a highly specific anti-CEA chimeric mAb (ch511) conjugated to a fluorophore in the 700-nm range (BM104). Clinical grade SGM-101 was obtained from SurgiMab (7). First, SGM-101 was dialyzed for 5 days in a Slide-A-Lyzer (10-kDa cutoff; Pierce Biotechnology Inc) against a 0.5 mol/L PBS solution. Subsequently, SCN-Bz-DTPA (Macrocyclics) was added in a 3-fold molar excess in DMSO. After 1 hour of incubation at room temperature on an orbital shaker in the dark, the reaction mixture was dialyzed for 5 days in a Slide-A-Lyzer (10-kDa cutoff; Pierce Biotechnology Inc) against PBS. The final concentration of the new conjugate was determined spectrophotometrically at 280 nm using an Infinite M200 Pro Multimode Reader (Tecan Group Ltd). The optical properties of both the SGM-101 starting material and the new conjugate were investigated. Absorbance and fluorescence spectra of both solutions were determined using the Infinite M200 Pro multimode reader. Radiolabeling of the new DTPA-SGM-101 with ^{111}In was done (see below) before and after dialysis to calculate the conjugation ratio of the chelator DTPA to SGM-101. High-performance liquid chromatography analysis of the radiolabeled conjugate was performed to determine the radiochemical purity of the new compound.

Radiolabeling and quality control of DTPA-SGM-101

For the first two biodistribution experiments on mice with subcutaneous tumors, DTPA-SGM-101 was labeled with 0.5 MBq of ^{111}In (Curium) in 0.5 mol/L 2-(N-morpholino) ethanesulfonic acid buffer, pH 5.4 (two times the volume of the [^{111}In]$InCl_3$ solution), and incubated for 20 minutes at room temperature under metal-free conditions. For studies where SPECT/CT was performed, DTPA-SGM-101 was radiolabeled with 10 MBq of ^{111}In per mice under similar conditions. Subsequently, 50 mmol/L ethylenediamine tetraacetic acid (EDTA) solution was added (final concentration, 5 mmol/L) to chelate unincorporated ^{111}In. Final labeling efficiency of the compound was determined by instant thin-layer chromatography on Silica Gel Strips (Agilent Technologies), where a 0.15 mol/L citrate buffer with pH 6.0 was used as mobile phase. The labeling efficiency exceeded 98% for all experiments.

The immunoreactivity of [^{111}In]In-DTPA-SGM-101 was determined with LS174T cells, as described by Lindmo and colleagues (14). Briefly, a serial dilution of LS174T cells was incubated with [^{111}In]In-DTPA-SGM-101 for 30 minutes at 37°C. Subsequently, cells were centrifuged and analyzed in a shielded 3″-well-type γ-Counter (PerkinElmer). The LS174T colorectal cancer cells used in all experiments were originally acquired from the ATCC (Batch F-9126). Cells were last tested for *Mycoplasma* in January 2018. All experiments were conducted within 1–2 months after thawing.

Tumor models

All animal experiments were conducted with 6- to 8-week-old female athymic BALB/c nu/nu mice (Janvier) weighing 20–25 g. Mice were given at least 1 week to become accustomed to laboratory conditions before starting with the experiments. Mice were housed in individually ventilated filter topped cages under nonsterile standard conditions with free access to chlorophyll-free chow and water in accordance with institutional guidelines. The subcutaneous tumors were induced by subcutaneous injection of 3×10^5 LS174T cells in 200 μL of RPMI1640 Medium (Gibco, Thermo Fischer Scientific) in the right flank of the mice. Intraperitoneal tumors were induced as described previously by Koppe and colleagues (15). In summary, mice were injected intraperitoneally with 10^6 LS174T cells suspended in 300 μL of RPMI1640 medium. Experiments were continued 1–2 weeks after tumor cell injection.

SPECT/CT and fluorescence imaging

SPECT/CT and fluorescence imaging were performed as described previously by Rijpkema and colleagues (16). In summary, SPECT/CT images were acquired with the U-SPECT-IICT System (MILabs). Mice were imaged for two frames of 25 minutes using a 1.0-mm diameter pinhole collimator, followed by a CT scan for anatomic referencing (spatial resolution, 160 μm; 65 kV; 612 μA). All scans were reconstructed with software supplied by MILabs, using an ordered subset expectation maximization algorithm with a voxel size of 0.375 mm.

SPECT/CT images were subsequently analyzed and created using the Inveon Research Workplace Software (IRW, version 4.1). Fluorescence images were acquired with an *In Vivo* Imaging System (Xenogen VivoVision IVIS Lumina II; Caliper Life Sciences). The acquisition time was 1–2 minutes with the following parameters: F/stop 2; binning medium; field of view C; excitation filter, 605 nm; and emission filter, 695–770 nm. Correction for autofluorescence was performed using a second acquisition of 10 seconds with an excitation filter of 605 nm.

IHC

IHC was performed as described by Elekonawo and colleagues (17). Slides were deparaffinized with xylene, rehydrated in ethanol, and rinsed in distilled water according to standard local protocol. Heat-induced antigen retrieval was performed in EDTA solution (pH 9.0). Endogenous peroxidase activity was blocked with 3% H_2O_2 in 10 mmol/L PBS for 10 minutes at room temperature. Subsequently, tissue sections were washed with 10 mmol/L PBS and stained with primary antibodies (CEA: Mouse monoclonal; Clone COL-1; MS-613-P; Neomarkers). Next, sections were incubated with biotin-free Poly-HRP-anti-mouse/rabbit IgG (ImmunoLogic/VWR International B. V.) in EnVision FLEX Wash Buffer (Dako Denmark A/S; 1:1) at room temperature for 30 minutes. Antibody binding was visualized using the EnVision FLEX Working Solution (Dako Denmark A/S) at room temperature for 10 minutes. All sections were counterstained with hematoxylin for 5 seconds and subsequently dehydrated in ethanol and coverslipped.

Ethical approval

All animal experiments were approved by the Animal Welfare Committee of the Radboud University Medical Center (Nijmegen, the Netherlands, local code: 2015-0071-147) and were conducted in accordance with the Revised Dutch Act on Animal Experimentation (Wet op de Dierproeven). The experiments involving the use of surgically derived human tissue samples were carried out according to the principles of the Declaration of Helsinki. The study protocol and collection of tissue were approved by the research ethics committee of the region Arnhem-Nijmegen (CMO regio Arnhem-Nijmegen, file code 2019-5437).

In vivo experiments

Dose escalation study

Mice with subcutaneous LS174T tumors in their right flank received an intravenous injection of 3, 10, 30, or 100 μg of [^{111}In]In-DTPA-SGM-101 per mouse (5 mice/group). A fifth group received 30 μg of radiolabeled [^{111}In]In-DTPA-SGM-101 complemented with 1 mg of unlabeled DTPA-SGM-101 as control group. Three days after injection of [^{111}In]In-DTPA-SGM-101, mice were euthanized using O_2/CO_2 asphyxiation, and blood, lung, heart, spleen, pancreas, stomach, small intestine, kidney, liver, muscle, and tumor were dissected and weighed. Activity in all resected specimens was measured in a Gamma-Counter (2480 WIZARD2; PerkinElmer). To calculate the uptake of radiolabeled antibodies in each sample as a fraction of the injected activity, aliquots of the injected dose were counted simultaneously. The results were expressed as percentage injected activity per gram (%IA/g).

Optimal timepoint determination

Mice with subcutaneous LS174T tumors received the optimal protein dose of 30 μg (as determined in the previous dose escalation study) of [^{111}In]In-DTPA-SGM-101 (10 MBq per mouse). After 24, 48, or 72 hours (5 mice at each timepoint), SPECT/CT and fluorescence imaging were performed as described above. Subsequently, mice were euthanized and the biodistribution of the radiolabel was determined as described in the previous experiment to assess the optimal timepoint for imaging after administration of the dual-labeled tracer.

Preoperative SPECT and fluorescence image–guided surgery study

Using the optimal conditions, as determined in the first two *in vivo* studies, multimodal image-guided surgery was performed in mice with intraperitoneally growing LS174T tumors as described previously by Rijpkema and colleagues (16). Mice received 30 μg of [^{111}In]In-DTPA-SGM-101 (10 MBq per mouse; 4 mice) or 30 μg of [^{111}In]In-DTPA-SGM-101 (10MBq per mouse, 2 mice) with 1 mg of unlabeled DTPA-SGM-101 that served as a negative control. Three days after administration of the antibody conjugate, preoperative SPECT/CT images were acquired, followed by fluorescence imaging (as described above) of the mice in supine position after surgical relocation of skin, abdominal muscle layers, and peritoneum. Subsequently, the visualized tumor nodules were resected and fluorescence imaging was repeated to check for residual tumor tissue. This procedure was repeated until all tumor nodules were removed.

Ex vivo incubation of fresh patient-derived peritoneal tumor samples

Finally, a translational experiment was conducted to assess tumor-to-surrounding (normal) tissue contrast in human tissue samples using fluorescence imaging and autoradiography as described previously by Elekonawo and colleagues (17). Fresh, surgically obtained peritoneal colorectal cancer deposits were incubated in tissue culture medium containing the tracer, [^{111}In]In-DTPA-SGM-101. Immediately after surgical resection, colorectal peritoneal tumor deposits were acquired and subsequently incubated overnight at 37°C in DMEM supplemented with 1% penicillin/streptomycin and 0.1% BSA (Sigma-Aldrich Chemie N.V.) and 4 μg/mL [^{111}In]In-DTPA-SGM-101 (0.05 MBg/μg). After overnight incubation, tumor deposits were washed in at least 3 L of continuously moving serially refreshed PBS supplemented with 0.1% BSA at 4–8°C for a minimum of 6 hours. Specimens were subsequently fixed in formalin and embedded in paraffin. Tissue sections (4-μm thick) were cut and placed on glass slides. Fluorescence images were acquired on a closed field Fluorescence Imaging System (Odyssey CLx; LI-COR Biosciences). Slides were then placed on a photostimulable phosphor plate. After 7 days, we imaged the plate on a Phosphor Imager (Typhoon FLA 7000 Phosphor Imager, GE Healthcare). Subsequently, slides were stained with hematoxylin and eosin (H&E) and IHC of CEA (mouse monoclonal; Clone COL-1; MS-613-P; Neomarkers) was performed. Surgical specimens from 2 patients received a nonspecific hIgG antibody-conjugate (SouthernBiotech) as negative controls. An independent pathologist reviewed the H&E and CEA slides to verify the presence and location of tumor cells. Regions of interest (ROI; tumor and adjacent normal tissue) were drawn in the corresponding fluorescence and autoradiography images to determine tumor-to-background ratios of both fluorescence and radiosignal.

Statistical analysis

Statistical analyses were performed using SPSS Statistics 25.0 (IBM) and GraphPad Prism Software (version 5.03; GraphPad Software). Tissue uptake at the different protein dose levels and timepoints was tested for significance using a one-way ANOVA test with *post hoc* Bonferroni correction. To test for differences in tumor and normal fluorescence and autoradiography intensities, a Mann–Whitney U test was used. Mean tumor-to-background ratios of the experimental

group were compared with mean tumor-to-background ratios in the control groups with an independent samples *t* test. An $\alpha < 0.05$ was considered to be statistically significant in all analyses.

Results

Comparison of SGM-101 and DTPA-SGM-101 showed similar patterns of absorbance and fluorescence emission before and after conjugation to the chelator (Supplementary Fig. S1). The substitution ratio of SGM-101 and DTPA was 1. The immunoreactive fraction of all conjugates exceeded 80% and radiochemical purity of [^{111}In]In-DTPA-SGM-101 used in all studies was >99%.

In the dose-escalation study, [^{111}In]In-DTPA-SGM-101 specifically accumulated in the subcutaneous CEA-positive LS174T tumors, with mean tumor uptake of 56.3 ± 14.2, 42.5 ± 15.1, 46.2 ± 6.7, and 21%IA/g ± 1%IA/g after injection of 3, 10, 30, and 100 μg, respectively. Tumor-to-blood ratios of mice that were injected with 3, 10, 30, or 100 μg were 5.6 ± 1.3, 5.0 ± 0.9, 5.8 ± 1.1, and 2.3 ± 0.4, respectively. Adding an excess of 1 mg unlabeled DTPA-SGM-101 decreased tumor uptake to 5.3%IA/g ± 0.4%IA/g and the tumor-to-blood ratio to 0.53%IA/g ± 0.2%IA/g, illustrating that tumor uptake of [^{111}In]In-DTPA-SGM-101 was specific. On the basis of these results, 30 μg was chosen as the optimal dose for subsequent experiments. Results of the biodistribution are summarized in **Fig. 1**.

In the second study, SPECT/CT imaging, NIR-fluorescence imaging, and biodistribution studies were performed 24, 48, and 72 hours after administration. Tumor uptake was 34.5 ± 5.4, 42.0 ± 16.1, and 56.4%IA/g ± 13.9%IA/g after 24, 48, and 72 hours, respectively. Tumor-to-blood ratios were 2.5 ± 0.5 after 24 hours, 3.7 ± 0.8 after 48 hours, and 5.1 ± 1.0 after 72 hours. Tumors could be visualized with both SPECT and fluorescence imaging at each timepoint. Seventy-two hours after administration of [^{111}In]In-DTPA-SGM-101 was chosen as the optimal timepoint for the imaging of peritoneal tumors in the next experiment. The results of this study, determining the optimal timepoint, are summarized in Supplementary Fig. S2.

In the third *in vivo* experiment, we performed preoperative SPECT/CT imaging and fluorescence-guided resection of tumor deposits in mice with intraperitoneally growing tumors. First, SPECT/CT images were acquired to visualize the extent of peritoneal disease dissemination. Subsequently, mice were euthanized, and laparotomy was performed to search for tumor deposits. After suspected tumors were found, by combining visual inspection and SPECT/CT imaging, fluorescence images were acquired and tumors were resected. **Figure 2** shows that after resection of all macroscopically visible tumors, fluorescence imaging revealed submillimeter tumor deposits that were initially missed by visual inspection. Mice that received the optimal dose with the addition of 1 mg unlabeled DTPA-SGM-101 did not show any specific accumulation of the tracer in the tumor on both imaging modalities (fluorescence imaging and SPECT). IHC analysis showed clear concordance between CEA-expressing tumor cells, fluorescence, and radiosignal (Supplementary Fig. S3).

In a final translational experiment, we collected 43 peritoneal deposits from 11 patients (three males and eight females). Median age was 76 (65–78) years. Seven patients were diagnosed with a peritoneally metastasized adenocarcinoma. In 1 patient, the peritoneal metastases originated from a mucinous adenocarcinoma and in another patient from a signet ring cell carcinoma. In one case, the peritoneal deposits contained a low-grade appendiceal mucinous neoplasm (LAMN), and another case was of an epithelial ovarian cancer. These last two cases did not express CEA and were used as negative controls.

After the incubation experiment, subsequent series of slides were produced from the surgically resected tumor deposits. This resulted in 43 series of slides that were analyzed. Thirty-three of the resected peritoneal deposits contained malignant cells. The other 10 lesions did not contain vital malignant tumor cells and consisted of fibrosis, necrosis, mucin, stroma, or fat. Median fluorescence intensity was 1,371 [interquartile range (IQR), 1,020–1,834] in tumors. This was significantly higher compared with adjacent normal tissue (fat, peritoneum, or stroma) where the median fluorescence intensity was 293 (IQR, 168–317; $P < 0.001$). Median intensity of the autoradiography for tumor tissue was 10.46×10^6 (IQR, 5.192×10^6 to 14.66×10^6). The median autoradiography intensity in adjacent nontumor tissue was 1.913×10^6 (IQR, 1.142×10^6 to 2.724×10^6; $P < 0.001$). Tumor-to-background ratios for the fluorescence and radiosignal of all cases are shown in **Fig. 3**. Fluorescence- and radiosignal-based tumor-to-background ratios were significantly lower in the CEA-negative cancers (no radiography data available for the LAMN

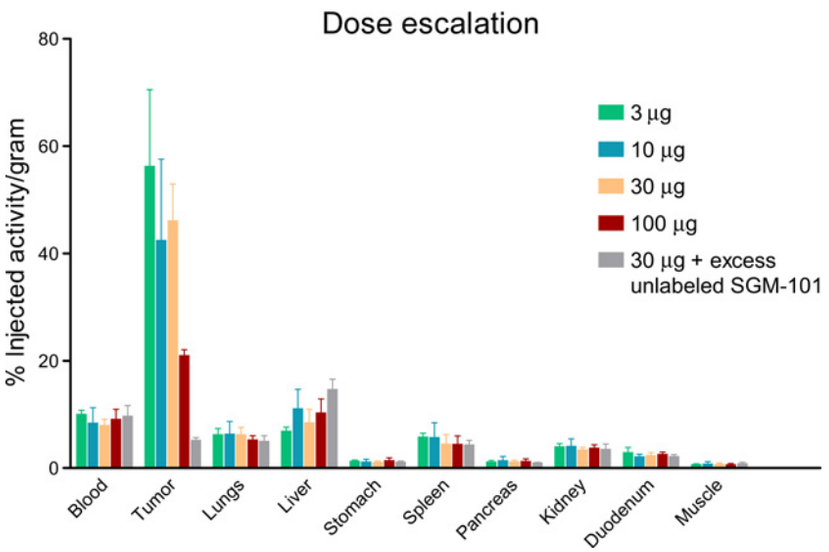

Figure 1.
Biodistribution of four different dose levels of [^{111}In]In-DTPA-SGM-101 in mice ($n = 5$ per dose level) with subcutaneous LS174T tumors. One group received a dose with an excess of 1 mg of unlabeled DTPA-SGM-101 as control group (gray, $n = 5$).

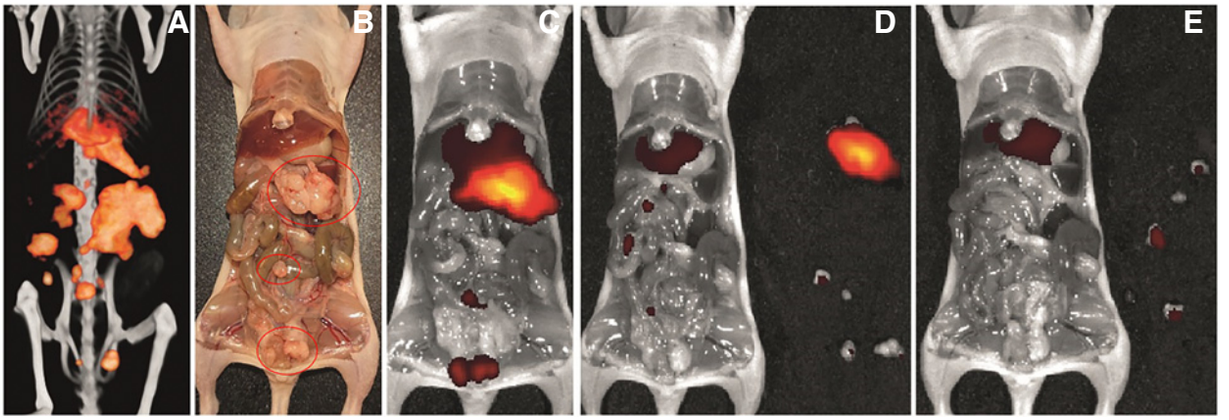

Figure 2.

A, SPECT/CT imaging shows extensive metastatic disease within the abdominal cavity in a mouse with intraperitoneally induced tumors. **B,** After surgical exposure, several tumor deposits were visible. **C** and **D,** Fluorescence imaging shows that after resection of macroscopically visible lesions, several tumor deposits remain present within the abdominal cavity. **E,** After fluorescence-guided resection is performed, no additional lesions are visible within the abdominal cavity and only physiologic uptake of the tracer in the liver remains.

due to a technical failure) and in the control cases incubated with the aspecific hIgG ($P < 0.001$ for both signals). Three examples of slides (H&E, CEA, and fluorescence and autoradiography) are provided in **Fig. 4**, illustrating the concordance between CEA-positive tumor cells and fluorescence and radiosignal. Microscopic images at a higher magnification confirming colocalization of CEA-expressing tumor cells and the fluorescence signal are shown in Supplementary Fig. S4.

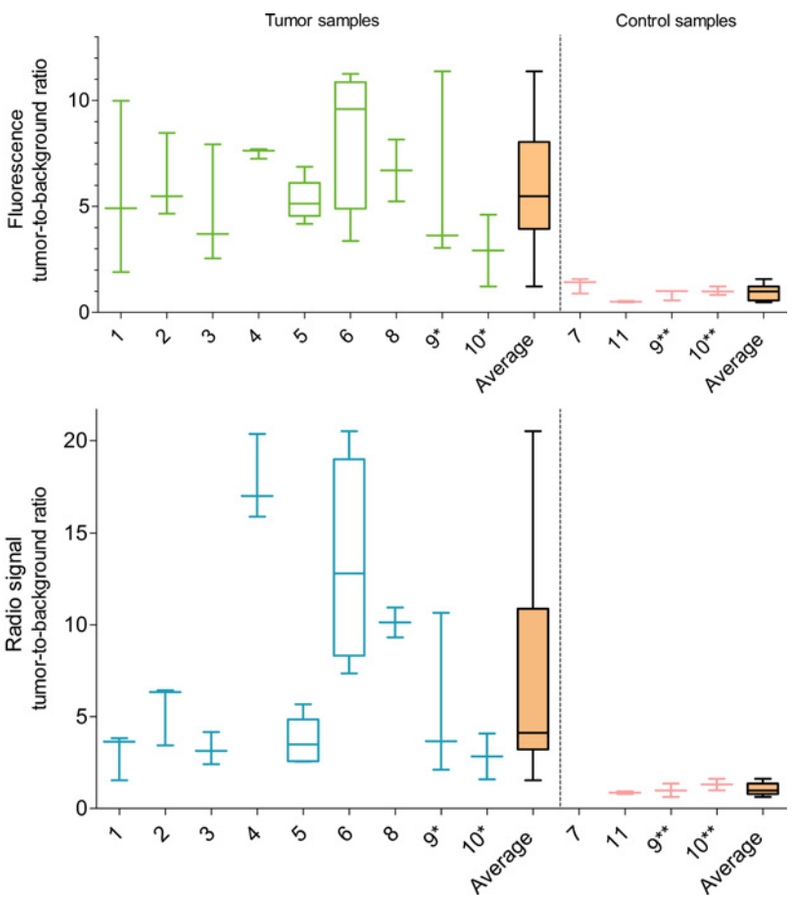

Figure 3.

Fluorescence-based (green, top graph) and radiosignal-based (blue, bottom graph) tumor-to-background ratios after incubation of surgically obtained tissue specimens. Tumor deposits from cases 9 and 10 were cut in half; each corresponding half was incubated with [^{111}In]In-DTPA-SGM-101 (9* and 10*) or an aspecific [^{111}In]In-DTPA-IgG-Cy5.5 (9** and 10**). Case 7 was a CEA-negative malignancy (LAMN). Average tumor-to-background ratios are shown in orange.

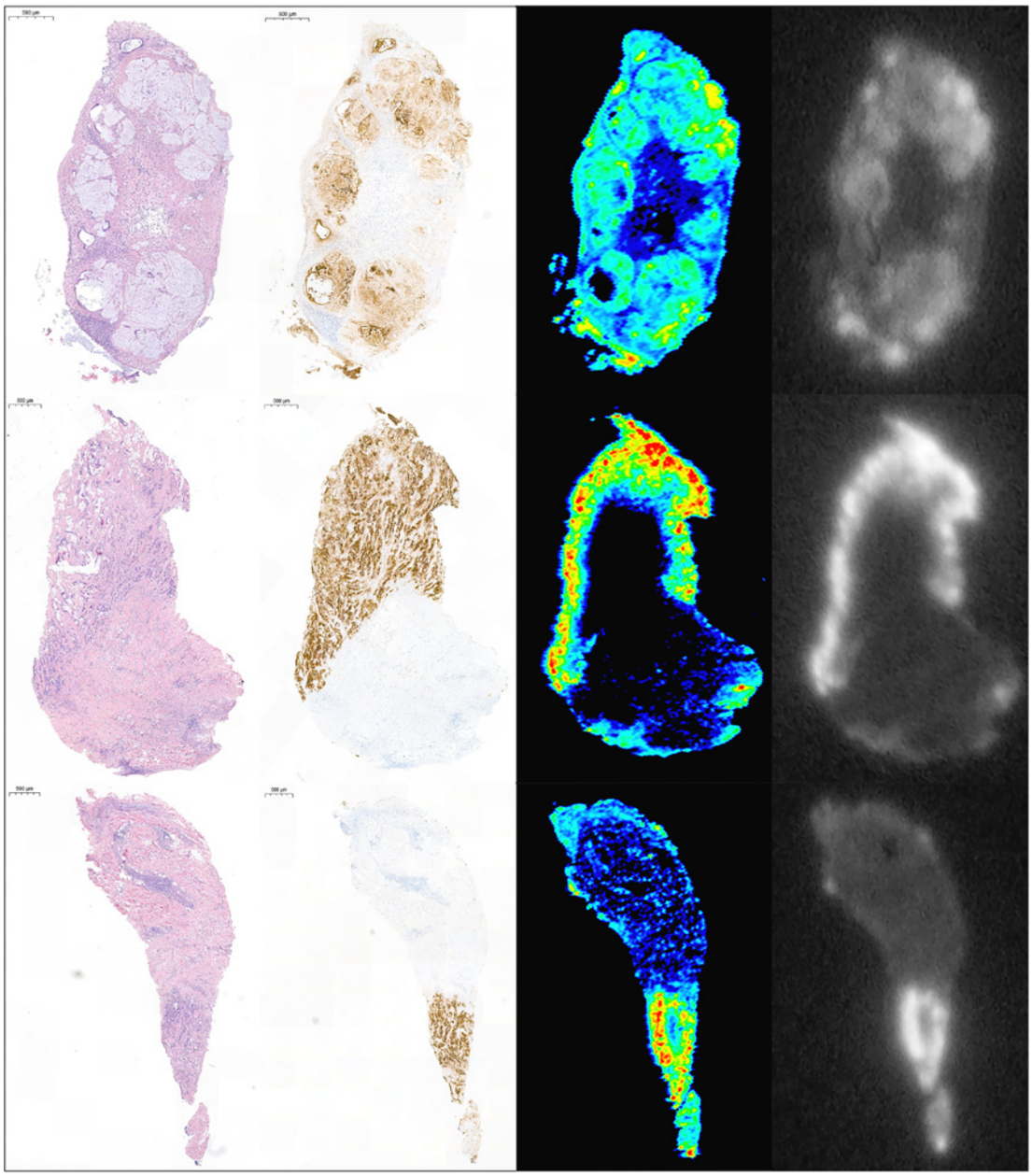

Figure 4.
Three examples of slides from the *ex vivo* incubation experiment on human tissues. H&E staining, CEA staining, and NIR fluorescence and autoradiography (left to right). Clear colocalization of CEA-expressing tumor cells and both fluorescence and radiosignal are observed.

Discussion

This study shows the *in vitro* and *in vivo* characterization of [^{111}In]In-DTPA-SGM-101 and the feasibility of multimodal image-guided surgery using this tracer. Accumulation of [^{111}In]In-DTPA-SGM-101 was high and specific in subcutaneous and peritoneal CEA-expressing LS174T xenografts. The biodistribution of this ^{111}In-labeled fluorescent tracer showed high tumor-to-blood ratios and low uptake in other organs. Translational *ex vivo* incubation studies with fresh surgically derived human peritoneal colorectal cancer deposits showed high tumor-to-background ratios and overall correspondence of both the fluorescence and radiosignal, suggesting the feasibility of this tracer for multimodal image-guided surgery of CEA-expressing colorectal cancer, warranting further evaluation in clinical studies.

The biodistribution of SGM-101 has been extensively investigated by Gutowski and colleagues in a similar colorectal cancer model (7). The reported results show a highly similar *in vivo* distribution of the tracer, with high uptake in the tumor compared with other tissues. As

expected, conjugation of DTPA to SGM-101 and subsequent radiolabeling with ^{111}In did not affect the *in vivo* behavior and distribution of SGM-101, as in accordance with the literature (18–20). The substitution ratio of DTPA to SGM-101 in our study was 1, which proved sufficient for radiolabeling in all experiments. Most chelating molecules can be conjugated to full IgG antibodies in ratios of up to 5 without significantly influencing or altering the immunoreactivity and *in vivo* behavior of the antibody (18–20). Because the *in vivo* behavior of iodinated SGM-101 and [^{111}In]In-DTPA-SGM-101 is comparable, [^{111}In]In-DTPA-SGM-101 could be used for quantification of tracer in tissue and blood, facilitating pharmacokinetic analysis of SGM-101 in a clinical setting.

In addition to accurate tracer quantification and pharmacokinetic analysis, intravenous injection of this dual-labeled tracer could facilitate clinical decision-making by improving preoperative tumor imaging. Whole-body SPECT/CT imaging might be used as an additional tool for noninvasive preoperative staging of the primary tumor, distant metastases, and lymph node metastases in patients with colorectal cancer, potentially adding to improved selection of patients with peritoneal metastases who are eligible for cytoreductive surgery and hyperthermic intraperitoneal chemotherapy. Conventional imaging modalities tend to underestimate the degree of intraperitoneal tumor extent in these patients (21). As a result of this underestimation, surgical procedures are performed on patients that are diagnosed with irresectable disease after surgical exploration of the abdomen, resulting in futile laparotomies or incomplete cytoreduction (21–24). SGM-101 fluorescence-guided cytoreductive surgery for colorectal peritoneal carcinomatosis has already been tested in a multicenter pilot study, and in one third of all cases, detection of additional malignant lesions by fluorescence imaging led to an adjustment of the peritoneal carcinomatosis index (25). Preoperative SPECT/CT imaging might also be used as a diagnostic aid to determine whether patients have extra-abdominal disease. Current criteria for determining whether lymph nodes or lung nodules are malignant are mainly based on size and morphologic features. A tumor-targeted molecular imaging approach might be valuable in determining whether lymph nodes and lung nodules that are considered borderline on conventional CT are malignant or benign. Combining these benefits of fluorescence-guided surgery with the additional value of a radiolabel could potentially improve diagnosis and treatment of these patients even further and will be evaluated in a clinical trial.

Another potential application of preoperative SPECT/CT imaging is the evaluation of metastatic lymph node status in patients with rectal cancer after preoperative radiation-based treatment. The current imaging modality of choice for determining the lymph node status is MRI, but reported sensitivity is low (26). CEA-targeted preoperative SPECT/CT could potentially be used as a restaging modality after neoadjuvant (chemo)radiotherapy because CEA expression is not influenced by neoadjuvant treatment (27). Subsequently, if patients exhibit tracer uptake in lymph nodes outside the standard total mesorectal resection specimen, such as lateral pelvic lymph nodes, radioguidance with a gamma probe could perhaps aid in localizing these lymph nodes. Subsequent intraoperative real-time fluorescence imaging could also help the surgeon in performing a complete resection of all metastatic lymph nodes and the primary tumor.

Besides colorectal cancer, combined CEA-targeted radioguidance and fluorescence imaging can potentially be translated to other CEA-expressing malignancies as well. De Gouw and colleagues have shown that 68% of lymph node metastases of esophageal cancer express CEA (28). Approximately one third of all surgically treated patients with esophageal cancer have lymph node metastases after neoadjuvant treatment, but lymphadenectomy is always performed because adequate treatment response assessment of lymph node metastases is not possible with current imaging modalities (29). CEA-targeted multimodal imaging might aid in minimizing or possibly omitting this procedure and reducing the associated morbidity in selected cases. The same hypothesis is worth investigating in gastric cancer, where similar dilemmas exist (30). CEA-targeted multimodal imaging could be investigated as a potential aid in identifying additional metastatic lymph nodes outside of the standard resection plane. It might also guide the surgeon in deciding to perform a less invasive D1 lymph node dissection instead of the more extensive D2 dissection, which is associated with increased morbidity (31, 32). In pancreatic cancer, fluorescence-guided surgery with SGM-101 was successful despite suboptimal intrinsic characteristics, such as poor vascularization, abundant presence of desmoplastic stroma, and localization of solitary ducts of tumor cells within benign pancreatic tissue (33). However, tumor-to-background ratios were lower as compared with colorectal cancer (9, 33). The addition of a radiolabel could be of added value when performing CEA-targeted image-guided surgery in these patients, similar to Hekman and colleagues, who successfully translated this approach of multimodal tumor-targeted image-guided surgery into the clinic (10, 34). In a first clinical study, they demonstrated the feasibility of combining preoperative SPECT/CT imaging, intraoperative gamma probe detection, and NIR fluorescence-guided surgery in patients with clear cell renal cell carcinoma (10).

There are some limitations to this study that need to be addressed. First, a mouse model with human colorectal cancer xenografts was used and one should consider that CEA expression may be more heterogeneous in a clinical setting. Because we did not use transgenic human CEA-expressing mouse models, tumor-to-background ratios will not be directly translatable to the clinical setting. However, in the preclinical toxicology study, the biodistribution of iodinated SGM-101 did not differ significantly between transgenic CEA-expressing mice and wild-type animals because physiologic CEA expression is exclusively located on the apical side of healthy epithelial cells, which is also the case with intestinal CEA expression in humans (8, 35). Therefore, it is not accessible to circulating CEA-targeting molecules, as opposed to malignant colorectal tumors, where CEA is overexpressed on the entire cell surface at a 60-fold higher density (35, 36). Second, the translational experiment that was performed with surgically derived peritoneal tumor deposits relies on passive diffusion of the tracer into the tissue to establish adequate uptake and tumor-to-background ratios. Because passive diffusion of full IgG antibodies will only facilitate penetration of approximately 100 μm within 12–18 hours of incubation, the center of the tumor deposit may not be reached by the tracer (17). However, although tracer distribution after intravenous injection still has to be shown in the clinic, the edges and invasive margins of the tumor are the main ROIs in surgical oncology and these results show that sufficient tumor-to-background ratios were reached for both the radio- and the fluorescence signal. These results are comparable with the tumor-to-background ratios found in the clinical studies conducted with SGM-101 (9, 25, 33).

In conclusion, this study shows the feasibility of CEA-targeted multimodal SPECT/CT and fluorescence imaging using [^{111}In]In-DTPA-SGM-101 in colorectal cancer models. [^{111}In]In-DTPA-SGM-101 enables specific and sensitive detection of colorectal cancer lesions *in vivo* and specifically targets tumor lesions in fresh surgical samples of colorectal cancer. The addition of a gamma-emitting

radiolabel to SGM-101 enables straightforward quantification *in vivo* and may facilitate preoperative detection of tumors by SPECT/CT imaging. Subsequent radio-guided intraoperative localization of deeper seated lesions combined with CEA-targeted fluorescence-guided surgery might further benefit the surgical treatment of colorectal cancer and other CEA-expressing malignancies. These promising preclinical results and our experience with the fluorescent tracer in clinical trials will pave the way for rapid clinical translation. On the basis of our results, this new multimodal tracer will likely improve clinical decision-making by personalized precision surgery.

Disclosure of Potential Conflicts of Interest

A. Pèlegrin reports being a founder and stockholder in SurgiMab. B. Framery reports other from SurgiMab SAS (employee) outside the submitted work. F. Cailler is listed as a coinventor on a patent on SGM-101 that is owned by SurgiMab. No potential conflicts of interest were disclosed by the other authors.

Authors' Contributions

J.M. de Gooyer: Conceptualization, data curation, formal analysis, investigation, visualization, methodology, writing-original draft. **F.M.K. Elekonawo:** Validation, investigation, visualization, writing-review and editing. **D.L. Bos:** Supervision, investigation, methodology, writing-review and editing. **R.S. van der Post:** Investigation, methodology, writing-review and editing. **A. Pèlegrin:** Conceptualization, supervision, methodology, writing-review and editing. **B. Framery:** Conceptualization, supervision, methodology, writing-review and editing. **F. Cailler:** Conceptualization, methodology, project administration, writing-review and editing. **A.L. Vahrmeijer:** Conceptualization, supervision, validation, methodology, writing-review and editing. **J.H.W. de Wilt:** Conceptualization, supervision, investigation, methodology, project administration, writing-review and editing. **M. Rijpkema:** Conceptualization, resources, data curation, supervision, investigation, methodology, writing-review and editing.

Acknowledgments

The authors would like to thank Bianca Lemmers van de Weem and Karin de Haas-Cremers for the assistance with the animal experiments.

The costs of publication of this article were defrayed in part by the payment of page charges. This article must therefore be hereby marked *advertisement* in accordance with 18 U.S.C. Section 1734 solely to indicate this fact.

Received June 11, 2020; revised July 22, 2020; accepted September 2, 2020; published first September 8, 2020.

References

1. Bray F, Ferlay J, Soerjomataram I, Siegel RL, Torre LA, Jemal A. Global cancer statistics 2018: GLOBOCAN estimates of incidence and mortality worldwide for 36 cancers in 185 countries. CA Cancer J Clin 2018;68:394–424.
2. Verwaal VJ, van Ruth S, de Bree E, van Sloothen GW, van Tinteren H, Boot H, et al. Randomized trial of cytoreduction and hyperthermic intraperitoneal chemotherapy versus systemic chemotherapy and palliative surgery in patients with peritoneal carcinomatosis of colorectal cancer. J Clin Oncol 2003;21:3737–43.
3. Brown KGM, Solomon MJ, Koh CE. Pelvic exenteration surgery: the evolution of radical surgical techniques for advanced and recurrent pelvic malignancy. Dis Colon Rectum 2017;60:745–54.
4. Nagtegaal ID, Quirke P. What is the role for the circumferential margin in the modern treatment of rectal cancer? J Clin Oncol 2008;26:303–12.
5. Dresen RC, Kusters M, Daniels-Gooszen AW, Cappendijk VC, Nieuwenhuijzen GA, Kessels AG, et al. Absence of tumor invasion into pelvic structures in locally recurrent rectal cancer: prediction with preoperative MR imaging. Radiology 2010;256:143–50.
6. Hammarström S. The carcinoembryonic antigen (CEA) family: structures, suggested functions and expression in normal and malignant tissues. Semin Cancer Biol 1999;9:67–81.
7. Gutowski M, Framery B, Boonstra MC, Garambois V, Quenet F, Dumas K, et al. SGM-101: an innovative near-infrared dye-antibody conjugate that targets CEA for fluorescence-guided surgery. Surg Oncol 2017;26:153–62.
8. Framery B, Gutowski M, Dumas K, Evrard A, Muller N, Dubois V, et al. Toxicity and pharmacokinetic profile of SGM-101, a fluorescent anti-CEA chimeric antibody for fluorescence imaging of tumors in patients. Toxicol Rep 2019;6:409–15.
9. Boogerd LSF, Hoogstins CES, Schaap DP, Kusters M, Handgraaf HJM, van der Valk MJM, et al. Safety and effectiveness of SGM-101, a fluorescent antibody targeting carcinoembryonic antigen, for intraoperative detection of colorectal cancer: a dose-escalation pilot study. Lancet Gastroenterol Hepatol 2018;3:181–91.
10. Hekman MC, Rijpkema M, Muselaers CH, Oosterwijk E, Hulsbergen-Van de Kaa CA, Boerman OC, et al. Tumor-targeted dual-modality imaging to improve intraoperative visualization of clear cell renal cell carcinoma: a first in man study. Theranostics 2018;8:2161–70.
11. Hekman MCH, Rijpkema M, Bos DL, Oosterwijk E, Goldenberg DM, Mulders PFA, et al. Detection of micrometastases using SPECT/fluorescence dual-modality imaging in a CEA-expressing tumor model. J Nucl Med 2017;58:706–10.
12. Tummers WS, Warram JM, van den Berg NS, Miller SE, Swijnenburg RJ, Vahrmeijer AL, et al. Recommendations for reporting on emerging optical imaging agents to promote clinical approval. Theranostics 2018;8:5336–47.
13. Lutje S, Rijpkema M, Helfrich W, Oyen WJ, Boerman OC. Targeted radionuclide and fluorescence dual-modality imaging of cancer: preclinical advances and clinical translation. Mol Imaging Biolo 2014;16:747–55.
14. Lindmo T, Boven E, Cuttitta F, Fedorko J, Bunn PA Jr. Determination of the immunoreactive fraction of radiolabeled monoclonal antibodies by linear extrapolation to binding at infinite antigen excess. J Immunol Methods 1984;72:77–89.
15. Koppe MJ, Soede AC, Pels W, Oyen WJ, Goldenberg DM, Bleichrodt RP, et al. Experimental radioimmunotherapy of small peritoneal metastases of colorectal origin. In J Cancer 2003;106:965–72.
16. Rijpkema M, Oyen WJ, Bos D, Franssen GM, Goldenberg DM, Boerman OC. SPECT- and fluorescence image-guided surgery using a dual-labeled carcinoembryonic antigen-targeting antibody. J Nucl Med 2014;55:1519–24.
17. Elekonawo FMK, de Gooyer JM, Bos DL, Goldenberg DM, Boerman OC, Brosens LAA, et al. *Ex vivo* assessment of tumor-targeting fluorescent tracers for image-guided surgery. Cancers 2020;12:987.
18. Kukis DL, DeNardo GL, DeNardo SJ, Mirick GR, Miers LA, Greiner DP, et al. Effect of the extent of chelate substitution on the immunoreactivity and biodistribution of 2IT-BAT-Lym-1 immunoconjugates. Cancer Res 1995;55:878–84.
19. Al-Ejeh F, Darby JM, Thierry B, Brown MP. A simplified suite of methods to evaluate chelator conjugation of antibodies: effects on hydrodynamic radius and biodistribution. Nucl Med Biol 2009;36:395–402.
20. Lewis MR, Raubitschek A, Shively JE. A facile, water-soluble method for modification of proteins with DOTA. Use of elevated temperature and optimized pH to achieve high specific activity and high chelate stability in radiolabeled immunoconjugates. Bioconjug Chem 1994;5:565–76.
21. van Oudheusden TR, Braam HJ, Luyer MD, Wiezer MJ, van Ramshorst B, Nienhuijs SW, et al. Peritoneal cancer patients not suitable for cytoreductive surgery and HIPEC during explorative surgery: risk factors, treatment options, and prognosis. Ann Surg Oncol 2015;22:1236–42.
22. Iversen LH, Rasmussen PC, Laurberg S. Value of laparoscopy before cytoreductive surgery and hyperthermic intraperitoneal chemotherapy for peritoneal carcinomatosis. Br J Surg 2013;100:285–92.
23. Pomel C, Appleyard TL, Gouy S, Rouzier R, Elias D. The role of laparoscopy to evaluate candidates for complete cytoreduction of peritoneal carcinomatosis and hyperthermic intraperitoneal chemotherapy. Eur J Surg Oncol 2005;31:540–3.
24. de Bree E, Koops W, Kroger R, van Ruth S, Witkamp AJ, Zoetmulder FA. Peritoneal carcinomatosis from colorectal or appendiceal origin: correlation of preoperative CT with intraoperative findings and evaluation of interobserver agreement. J Surg Oncol 2004;86:64–73.
25. Schaap DP, de Valk KS, Deken MM, Meijer RPJ, Burggraaf J, Vahrmeijer AL, et al. Carcinoembryonic antigen-specific, fluorescent image-guided

cytoreductive surgery with hyperthermic intraperitoneal chemotherapy for metastatic colorectal cancer. Br J Surg 2020;107:334–7.
26. Brouwer NPM, Stijns RCH, Lemmens V, Nagtegaal ID, Beets-Tan RGH, Futterer JJ, et al. Clinical lymph node staging in colorectal cancer; a flip of the coin? Eur J Surg Oncol 2018;44:1241–6.
27. Boogerd LS, van der Valk MJ, Boonstra MC, Prevoo HA, Hilling DE, van de Velde CJ, et al. Biomarker expression in rectal cancer tissue before and after neoadjuvant therapy. Onco Targets Ther 2018;11:1655–64.
28. de Gouw D, Rijpkema M, de Bitter TJJ, Baart VM, Sier CFM, Hernot S, et al. Identifying biomarkers in lymph node metastases of esophageal adenocarcinoma for tumor-targeted imaging. Mol Diagn Ther 2020:24:191–200.
29. van Hagen P, Hulshof MC, van Lanschot JJ, Steyerberg EW, van Berge Henegouwen MI, Wijnhoven BP, et al. Preoperative chemoradiotherapy for esophageal or junctional cancer. N Engl J Med 2012;366:2074–84.
30. Vuijk FA, Hilling DE, Mieog JSD, Vahrmeijer AL. Fluorescent-guided surgery for sentinel lymph node detection in gastric cancer and carcinoembryonic antigen targeted fluorescent-guided surgery in colorectal and pancreatic cancer. J Surg Oncol 2018;118:315–23.
31. Cuschieri A, Fayers P, Fielding J, Craven J, Bancewicz J, Joypaul V, et al. Postoperative morbidity and mortality after D1 and D2 resections for gastric cancer: preliminary results of the MRC randomised controlled surgical trial. The Surgical Cooperative Group. Lancet 1996;347:995–9.
32. Bonenkamp JJ, Songun I, Hermans J, Sasako M, Welvaart K, Plukker JT, et al. Randomised comparison of morbidity after D1 and D2 dissection for gastric cancer in 996 Dutch patients. Lancet 1995;345:745–8.
33. Hoogstins CES, Boogerd LSF, Sibinga Mulder BG, Mieog JSD, Swijnenburg RJ, van de Velde CJH, et al. Image-guided surgery in patients with pancreatic cancer: first results of a clinical trial using SGM-101, a novel carcinoembryonic antigen-targeting, near-infrared fluorescent agent. Ann Surg Oncol 2018;25:3350–7.
34. Hekman MC, Boerman OC, de Weijert M, Bos DL, Oosterwijk E, Langenhuijsen JF, et al. Targeted dual-modality imaging in renal cell carcinoma: an *ex vivo* kidney perfusion study. Clin Cancer Res 2016;22:4634–42.
35. Jay P, Berta P, Blache P. Expression of the carcinoembryonic antigen gene is inhibited by SOX9 in human colon carcinoma cells. Cancer Rese 2005;65:2193–8.
36. Boonstra MC, de Geus SW, Prevoo HA, Hawinkels LJ, van de Velde CJ, Kuppen PJ, et al. Selecting targets for tumor imaging: an overview of cancer-associated membrane proteins. Biomark Cancer 2016;8:119–33.